*Anal. Chem.* **2010,** *82,* 9663–9670

# A Closed Form for Fluorescence Correlation Spectroscopy Experiments in Submicrometer Structures

**Luigi Sanguigno,*,†,§ Ilaria De Santo,†,‡ Filippo Causa,‡ and Paolo Netti†,‡**

*Centre for Advanced Biomaterials for Health Care, Italian Institute of Technology (IIT) and Department of Materials and Production Engineering and Interdisciplinary Research Centre on Biomaterials, University of Naples Federico II, P.le Tecchio 80, 80125 Naples, Italy, and Technological District in Polymer and Composite Engineering (IMAST Scarl), P.le Fermi 1, 80055, Portici, Naples, Italy*

**Fluorescence correlation spectroscopy (FCS) is a powerful technique for measuring low concentrations of fluorescent molecules and their diffusion coefficients in an open detection volume. However, in several practical cases, when FCS measurements are carried out in small compartments like microchannels, neglecting boundary effects could lead to erroneous results. Here, a close form solution is proposed to explicitly account for the presence of walls located at a distance comparable with the characteristic detection volume lengths. We derive a one-dimensional diffusion constrained model and then generalize the solution to the two- and the three-dimensional constrained cases. We further indicate within which limits the standard autocorrelation function (ACF) model gives reliable results in microconfinement. Our model relies just on the assumption of elastic hits at the system walls and succeeds in describing the ACF of fluorescent probes confined along one direction. Through the analysis of FCS experimental data, we are able to predict the correct shape of the ACF in channels of micrometric and submicrometric width and measure the extent of lateral confinement. In addition, it permits the investigation of microstructured material features such as cages and cavities having dimensions on the micrometric range. On the basis of the proposed model, we also show in which conditions confinement could generate an apparent time dependent probe mobility, thus allowing a proper interpretation of the transport process taking place in submicrometric compartments.**

Fluorescence correlation spectroscopy (FCS) has been extensively used in the past two decades to measure molecular diffusion in dilute solutions and on membranes and analyze chemical kinetics and conformational dynamics.[1] Although usually applied to freely diffusing molecules, FCS has been involved as a robust procedure for the measurement of molecular mobility in and on live cells and tissues. Indeed, FCS has been used to monitor the molecular motion in subcellular compartments such as molecule trafficking through calcium channels for secretion and synaptic transmission[2] and molecule transport within a patch clamp with a perforated vesicle containing calcium or potassium channels.[3] Recently, this technique has been applied to measure the diffusion coefficient and the convective flow of fluorescent probes in microcapillaries and submicrometer structures.[4−7]

In all the cases in which the mobility is measured in small compartments, the main limitation regarding FCS applicability is due to the lack of an adequate interpreting model since the ones available in the literature are suitable for infinite size systems. Generally, the deficiency of the convectional models occurs when FCS experiments are carried out inside systems comparable with the FCS focal volume which is less than one femtoliter. Strong deviations from widely established models were reported for molecular diffusion in the self-assembled lipid tubule interior[8] and membranes.[9]

In these not standard operative conditions, many formulations, either numerical[10−12] or statistical[13] have been proposed in order to predict the experimental autocorrelation function (ACF). Therefore, an extension of the standard ACF model (freely diffusing fluorescent probes) is largely required when fluorescent intensity fluctuations are measured in confined volumes. This extension should allow the usage of complex biophysical models accounting for several aspects such as the chemical nature of the

* To whom correspondence should be addressed. E-mail: lusangui@unina.it. Phone: +39 081 7682512. Fax: +39 081 7682404.

† Centre for Advanced Biomaterials for Health Care, Italian Institute of Technology (IIT), University of Naples Federico II.

‡ Department of Materials and Production Engineering and Interdisciplinary Research Centre on Biomaterials, University of Naples Federico II.

§ Technological District in Polymer and Composite Engineering (IMAST Scarl).

(1) Elson, E. L.; Magde, D. *Biopolymers* **1974**, *13*, 1–27.
(2) Gonzales, E. B.; Kawate, T.; Gouaux, E. *Nature* **2009**, *460*, 599–604.
(3) Levitan, E. S.; Kramer, R. H. *Nature* **1990**, *348*, 645–647.
(4) Dittrich, P. S.; Schwille, P. *Anal. Chem.* **2002**, *74*, 4472–4479.
(5) Lennes, P. F.; Colombo, D.; Giovannini, H.; Rigneault, H. *Single Mol.* **2002**, *3*, 194–200.
(6) Foquet, M.; Korlach, J.; Zipfel, W. R.; Webb, W. W.; Craighead, H. G. *Anal. Chem.* **2004**, *76*, 1618–1626.
(7) Petrasek, Z.; Krishnan, M.; Monch, I.; Schwille, P. *Microsc. Res. Tech.* **2007**, *70*, 459–466.
(8) Guo, L.; Chowdhury, P.; Fang, J.; Gai, F. *J. Phys. Chem. B* **2007**, *111*, 14244–14249.
(9) Ries, J.; Schwille, P. *Phys. Chem. Chem. Phys.* **2008**, *10*, 3487–3497.
(10) Gennerich, A.; Schild, D. *Biophys. J.* **2000**, *79*, 3294–3309.
(11) Feder, T.; Brust-Mascher, I.; Slattery, J.; Baird, B.; Webb, W. W. *Biophys. J.* **1996**, *70*, 2767–2773.
(12) Milon, S.; Hovius, R.; Vogel, H.; Wohland, T. *Chem. Phys.* **2003**, *39*, 171–186.
(13) Weiss, M.; Hashimoto, H.; Nilsson, T. *Biophys. J.* **2003**, *84*, 4043–4052.

10.1021/ac102084m 
Published on Web 11/01/2010

confinement and its environment. In this context, we proposed a versatile and easy tool that accounts for the presence of walls at a distance comparable to the characteristic lateral length of the focal volume. Assuming the walls are ideal reflectors, we are able to predict the ACF in submicrometric and micrometric structures and the confinement extension. We also indicate above which critical system size the wall effect can be conveniently neglected. Moreover, our method could be further extended to include more complex transport models and probe−wall interactions.

## STANDARD MODEL

FCS is based on the statistical analysis of fluorescence intensity fluctuations due to fluorescent probe trafficking in a small volume of the sample where light is focused (focal volume). The fluctuations are analyzed by temporal autocorrelation, and the resulting ACF can be predicted by averaging all possible fluorescent probe trajectories in a given time interval (lag time). Therefore, if the nature of the undergoing transport process is known and representable through a simple biophysical model, a theoretical ACF can be formulated and its prediction compared with experimental data. Generally, Brownian dynamics is assumed to be a reliable biophysical model for probe motion in a liquid. Brownian dynamics assumes that all moving probes are identical and independently moving from the others. In addition, probe displacements along at least three directions are assumed to be uncorrelated. On this basis, the standard ACF of the fluorescent intensity signal can be defined in terms of single particle average contribution,[1,14]

$$G(t) = \frac{1}{\langle i \rangle^2} \int \int I_E(\vec{r}_1) I_E(\vec{r}_2) p(\vec{r}_1, \vec{r}_2, t) d\vec{r}_1 d\vec{r}_2 \qquad (1)$$

where $\langle i \rangle$ is the average intensity, $I_E$ is detectable emission intensity distribution (spatial detectivity function), and $p$ is the probability density for a single particle that started a random walk at time 0 at the point $\vec{r}_1$ to be at $\vec{r}_2$ at a lag time $t$. $I_E$ depends on the FCS optical setup since it represents the effective shape of the detection volume. As suggested by Rigler,[15] the spatial detectivity function can reliably be approximated by a three-dimensional Gaussian profile,

$$I_E(\vec{r}) = I_0 e^{-2[(x^2+y^2)/r_{xy}^2]} e^{-2(z^2/r_z^2)} \qquad (2)$$

where $r_{xy}$ and $r_z$ are, respectively, the characteristic lengths of the detection volume. Under these assumptions, Aragón and Pecora[16] derived the following standard ACF expression,

$$G(t) = \frac{g(t)}{\langle i \rangle^2} = \frac{1}{\langle N \rangle} \frac{1}{\sqrt{1 + 4Dt/r_{xy}^2}} \frac{1}{\sqrt{1 + 4Dt/r_{xy}^2}} \frac{1}{\sqrt{1 + 4Dt/r_z^2}} \qquad (3)$$

where $D$ and $\langle N \rangle$ correspond to the probe diffusion coefficient and the average number of particles detected in the focal volume, respectively. The standard ACF model, eq 3, consists of the product of three identical functional forms representing the temporal autocorrelation contributions due to the probe displacement along the axial directions ($\hat{x}$, $\hat{y}$, and $\hat{z}$). This property comes directly from the assumption that particle paths along these directions are uncorrelated which permits one to decouple the double integral in eq 1 along the three axial directions. Decoupling ACF along the axial directions is valid as long as Brownian particles moving inside a 3D Gaussian detectivity function are taken into account. Therefore, a general form[17] of the ACF can be rewritten as

$$G(t) = \frac{1}{\langle N \rangle} \frac{g_x(t)}{g_x(0)} \frac{g_y(t)}{g_y(0)} \frac{g_z(t)}{g_z(0)} \qquad (4)$$

## DIFFUSION CONSTRAINED BY WALLS ALONG AXIAL DIRECTION

Whenever FCS measurements are carried out in systems having at least one dimension comparable to the characteristic length of the detection volume, the presence of lateral confinements, like walls, needs to be explicitly accounted for in order to properly estimate the probe mobility. Decoupling the ACF along the axial directions is valid as long as Brownian dynamics is assumed to be the transport mechanism forcing the probes to move within a 3D Gaussian detectivity function. Indeed, the presence of walls along the axial directions does not affect the applicability of the eq 4; thus, the constrains can still be considered independently along each direction. Therefore, the constrained diffusion problem is solved along a generic axial direction, $\hat{k}$, where the confinement is defined. In the case of interest, the detection volume characteristic length, $r_k$, is comparable with the system width, $d$, defined as the distance between two walls located at 0 and $d$, respectively, see Figure 1a. The ACF along the generic axial direction $\hat{k}$ is defined as

$$g_k(t) = \int_0^d \int_0^d e^{-2[(k_1-k_0)/r_k^2]} e^{-2[(k_2-k_0)/r_k^2]} p_c(k_1, k_2, t) dk_1 dk_2 \qquad (5)$$

where $k_0$ is the laser beam focus position with respect to the axes origin, $k_1$ and $k_2$ are the components of $\hat{r}_1$ and $\hat{r}_2$ along the $\hat{k}$ direction, and $p_c$ is the confined probability density function relative to displacements occurring along the $\hat{k}$ direction. The confined probability density could be represented by the 2D Fokker−Planck solution, as previously suggested by Gennerich and Schild[10] and by Elson and Madge.[1]

Here, an alternative treatment is proposed where the effect of lateral confinement on the ACF is modeled through the reflection and superposition method[18] which consists in folding the unconfined probability density function, $p$, within the system walls, Figure 2a. The constrained probability density, $p_c$, is obtained by summing up all the parts derived from the reflections of the unconfined probability density within the interval $[0,d]$. Due to the linearity of the integral operator, eq 5 can be rewritten as the sum of integrals each corresponding to a single reflection contribution. These contributions can be spatially rearranged as


(14) Papoulis, A. *Probability, Random Variables and Stochastic Processes*, 3rd ed.; McGraw-Hill Companies: New York, 1991.
(15) Rigler, R.; Mets, U.; Widengren, J.; Kask, P. *Eur. Biophys. J.* **2000**, *39*, 642–651.
(16) Aragon, S. R.; Pecora, R. *J. Chem. Phys.* **1976**, *64*, 1791–1803.
(17) Rigler, R.; Elson, E. S. *Fluorescence correlation spectroscopy: Genesis, Evolution, Maturation and Prognosis*, 2nd ed.; Springer: Heidelberg, Germany, 2001.
(18) Crank, J. *The mathematics of diffusion*, 2nd ed.; Oxford University Press: New York, 1975.

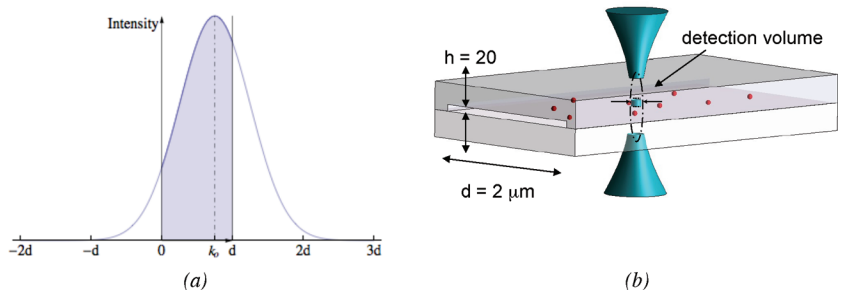


(a) (b)

**Figure 1.** Details on FCS measurements. (a) Gaussian detectivity distribution confined by walls located at 0 and $d$ (light blue area) along an arbitrary direction $\hat{k}$. $r_k$ represents the characteristic length of confocal volume along one direction centered at $k_0$. (b) Experimental setup used for FCS measurement in channels (not to scale). Structure of a channel with nanometric height of 20 nm and width of 2 $\mu$m. The sampling volume is confined approximately to a cylindrical volume of height $h$ and radius equal to the confocal waist $r_{xy}$. Molecules (in red) are detected while diffusing through the sampling volume.

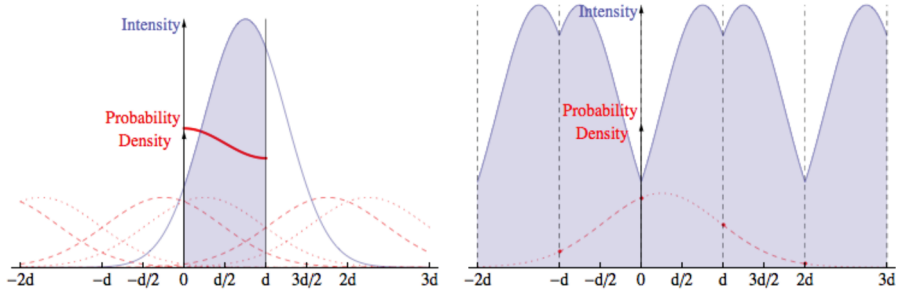


(a) (b)

**Figure 2.** Graphical representation of the mathematical equivalence between ACF of constrained diffusing particles (a) and ACF of an unconfined particle belonging to a periodic detectivity distribution (b). (a) The correlation is the integral from 0 to $d$ of the product of the Gaussian detectivity distribution and the confined probability density (tick line), which corresponds to the sum of reflected unconfined probability density functions needed to fold the probability density within the system walls (dotted and dashed lines). (b) The same result can be calculated as the product of the unconfined probability density (red dashed line) times the PD function obtained by consecutive reflections of the real detectivity function with respect to the walls (light blue area).

shown in Figure 2b resulting in a unique integral defined from $-\infty$ to $+\infty$. This integrates the product of the unconfined probability density and the periodic spatial detectivity function (PD) obtained by consecutive reflections of the real one with respect to the system walls, Figure 2b. This proves the equivalence of an ACF of a confined particle and that of an unconfined one moving below a PD function. Furthermore, the PD function, being symmetric with respect to the origin, can be represented by Fourier cosine series of amplitudes $a_n$ defined over the interval [0,2$d$]; see Figure 2b. This allows one to compute the ACF as

$$g_k(t) = \frac{d}{2}\left[\frac{a_0^2}{2} + \sum_{n=1}^{+\infty} a_n^2 e^{-(n^2\pi^2/2R^2)\,(t/t_d)}\right] \tag{6}$$

The parameter $R$ is a dimensionless number which is proportional to the system width, $d$, and is equal to $((2)^{1/2}d)/r_k$, while $t_d$ corresponds to the characteristic diffusion time which is defined as $r_k^2/(4D)$, coherently with the standard model. The analytical expression of $a_n$ is given below,

$$a_n = \frac{\sqrt{\pi}}{2R} e^{-(\pi^2 n^2/4R^2) - (iH_{n\pi}/R)}\left[\operatorname{erf}\left(H - \frac{in\pi}{2R}\right) - \operatorname{erf}\left(H - R - \frac{in\pi}{2R}\right) + e^{2iH_{n\pi}/R}\left(\operatorname{erf}\left(H + \frac{in\pi}{2R}\right) - \operatorname{erf}\left(H - R + \frac{in\pi}{2R}\right)\right)\right] \tag{7}$$

where $H$ is another dimensionless parameter equal to $((2)^{1/2}k_0)/r_k$ which represents the laser focus potion with respect to the walls. When this position corresponds to the system middle point ($k_0 = d/2$ or $H = R/2$), the $a_n$ expression results are strongly simplified and eq 7 becomes

$$a_n = \frac{\sqrt{\pi}}{R} e^{-(n^2\pi^2/4R^2)} \cos\left(\frac{n\pi}{2}\right)\left[\operatorname{erf}\left(\frac{in\pi}{2R} + \frac{R}{2}\right) - \operatorname{erf}\left(\frac{i\pi n}{2R} - \frac{R}{2}\right)\right] \tag{8}$$

thus reducing the mathematical expression complexity. In both equations, eqs 7 and 8, the highest computational cost is required by the calculation of error functions, erf, with complex arguments.[19] The operative ACF expression is then obtained by normalizing the $g_k(t)$ function respect to its initial value,

$$g_k(0) = \frac{r_k\sqrt{\pi}}{2}[\operatorname{erf}(\sqrt{2}(R - H)) + \operatorname{erf}(\sqrt{2}H)] \tag{9}$$

as previously determined in the standard model derivation procedure, eq 4. The strong simplification of the eq 8 is mainly due to the detectivity function shape which is further symmetric with respect to its focus. Indeed, when the laser focus is at the system center, the basic interval of the Fourier series changes from [0,2$d$] to [0,$d$], leading all $a_n$ coefficients evaluated at even values to be zero; see eq 7.

(19) Abramowitz, M.; Stegun, I. A. *Handbook of mathematical functions*, 2nd ed.; Dover Publications, Inc.: New York, 1972.

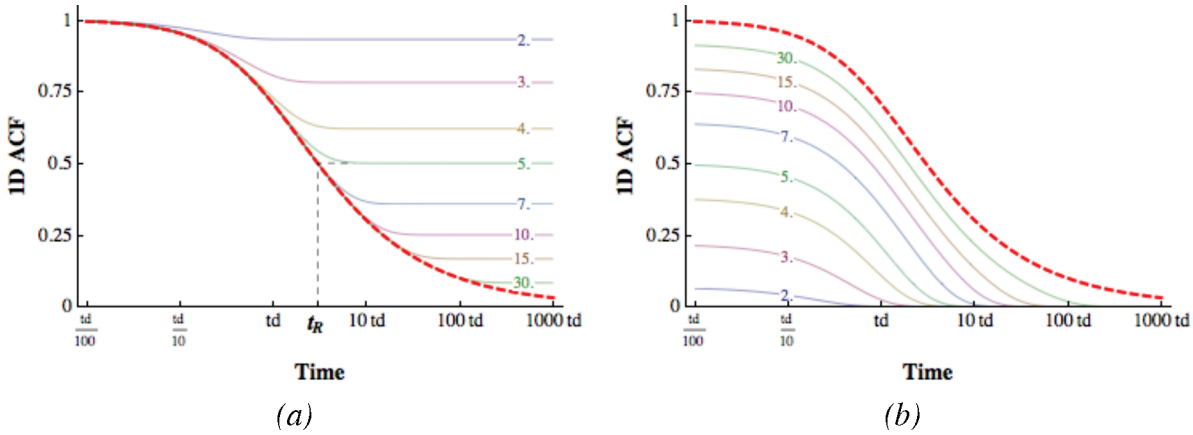


**Figure 3.** 1D confined ACF contribution at different values of $R = ((2)^{1/2}d)/r_k$ (full lines), compared with standard 1D ACF (dashed red line). (a) When $R$ values are decreased, the ACF contribution approaches a constant value equal to 1 since particle movements do not produce detectable signal fluctuations along the confined direction and, in turn, its contribution to the overall ACF is negligible. At increasing system size (higher $R$ values), the 1D ACF contribution asymptotically approaches the 1D standard contribution since the average time needed to collide with the walls becomes larger than the characteristic decorrelation time. (b) The ACF is forced to be zero at large lag since even in constrained systems fluctuations cannot persist endlessly. When $R$ values are reduced, 1D confined ACF approaches the zero function since intensity signal deviations from the mean value are almost zero.

## ONE-DIMENSIONAL SYMMETRICALLY CONFINED DIFFUSION

The effect of the confinement along the generic $\hat{k}$ direction is shown in Figure 3a, where $g_k(t)/g_k(0)$ is calculated for several system sizes, $R$. In each computed case, the model predicts the lag time $t_R$ at which the deviation from the standard ACF occurs. In large systems, $t_R$ becomes greater than the characteristic diffusion time, $t_d$; thus, the prediction converges on the standard ACF, and the wall effect is no longer significant. Mathematically, the constrained case and the standard model correspond until negligible reflections are required to realize the null flux condition at the walls. Therefore, $t_R$ corresponds to the average time between sequential particles−wall collisions; thus, when the system size is increased, the deviation occurs at larger $t_R$.

As shown in Figure 3a, the model predicts a plateau at large lag times for a generic constrained dimension. Indeed, the probability of finding a particle that starts a random walk at a given position to be elsewhere within the walls is finite even at large times. The plateau value is related to the highest possible mean square displacement (MSD), which is limited since the system is of finite size. Along a constrained direction, the correlation reaches a plateau without decaying to zero and, therefore, it might seem that a perturbation persists in a finite volume endlessly. Moreover, ACF becomes identically equal to 1 as the system size, $d$, approaches zero. This misconceptions are due to the unsuitability of eq 4 which has to be modified as

$$G(t) = \frac{1}{\langle N \rangle} \frac{g_x(t)g_y(t)g_z(t) - g_x(\infty)g_y(\infty)g_z(\infty)}{g_x(0)g_y(0)g_z(0)} \qquad (10)$$

to correctly describe the ACF in finite systems. In infinite systems, any kind of fluctuation, considered as an initial condition for the ACF prediction, becomes identically zero at large lag time and then is forgotten. On the contrary, in finite systems, the ACF decay to zero has to be imposed since is not guaranteed for all possible initial conditions. For symmetrically confined systems, the analytical expression of the large lag time plateau is again strongly simplified and becomes

$$\frac{g_k(\infty)}{g_k(0)} = \frac{\sqrt{2\pi}\,\mathrm{erf}(R/2)^2}{R\,\mathrm{erf}(R/\sqrt{2})} \qquad (11)$$

In Figure 3b, the effect of the confinement for one-dimensional constrained systems is illustrated, where $g_k(t)/g_k(0) - g_k(\infty)/g_k(0)$ is displayed at several $R$ values. As a result of eq 10, the ACF decays to zero for large lag times and low $R$ values. This observation agrees with what was attended for a zero size system where particles are unable to move and, thus, produce fluctuations.

## DIFFUSION MODEL WITH WALLS IN MORE THAN ONE DIMENSION

In order to generalize the solution to higher dimensional cases, eqs 4 and 10 have to be applied. Diffusion constrained in channels (2D) and boxes (3D) are again treated considering the focus located at the system middle point since this configuration is commonly adopted in nonstandard FCS measurements. The model predictions are shown for both cases and compared with the 1D and 3D standard ACF; see Figure 4.

In the case of fluorescent probes confined in the channel of several widths, all ACF curves are locked within the region defined by 3D and 1D standard ACF, Figure 4a. When the channel section is reduced, the confined ACF progressively approaches the standard 1D ACF. In general, for constrained systems, the decorrelation cannot occur faster than the 3D standard ACF and slower than 1D or 2D standard ACF depending on the number of directions along which the motion is confined. When the particle motion is confined along all directions, Figure 4b, the ACF strongly deviates from the 3D standard model in terms of both shape and initial value, since eq 10 is used instead of eq 4 to impose total decorrelation at large lag time. The accuracy of this correction is validated by the fact that ACF goes to the identically zero function with a reduction in system size, and this is in agreement with what is physically attended since the system is so small that fluctuations cannot occur any more in any direction.

## EXPERIMENTAL SETUP

Borosilicate channels manufactured by chemical etching and direct bonding procedures were used to register ACF deviations

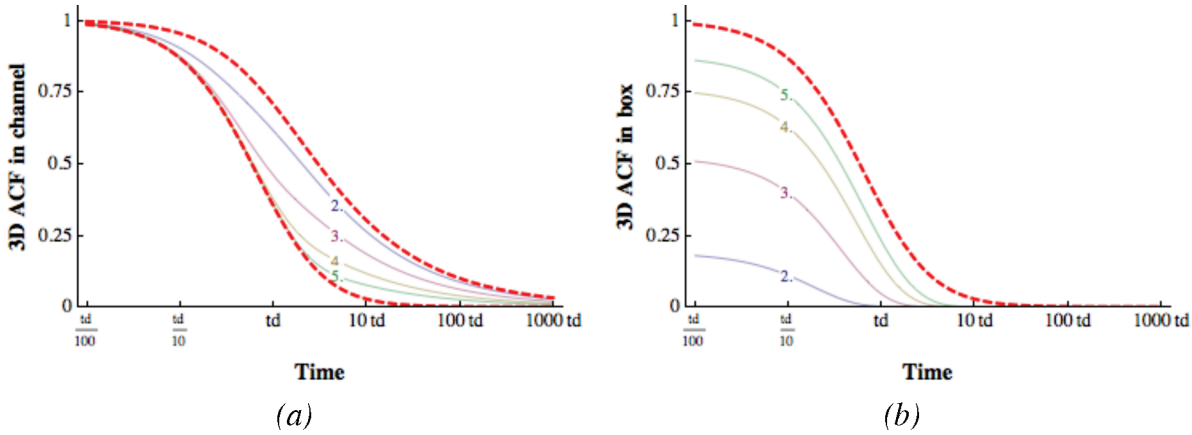


**Figure 4.** 3D ACF in a channel and in a box. (a) 3D ACF symmetrically constrained along *x* and *y* directions at different values of $R = R_x = R_y$ (full line) compared with standard 3D and 1D ACF (dashed lines). When the system size along two dimensions is reduced, the ACF deviates from the 3D ACF approaching the 1D curve. When the particle motion is symmetrically confined along two directions, the constrained ACF always lies within the 3D and 1D ACF. (b) 3D ACF symmetrically constrained along all directions at different values of $R = R_x = R_y = R_z$ (full lines) compared with the 3D ACF (dashed line). When the system size along all directions is reduced, the ACF decorrelates faster than the 3D standard case and it approaches zero when the system becomes so small that particle movements are confined on a scale where intensity signal fluctuations are negligible.

in confined systems (Micronit Microfluidics, Enschede, The Netherlands).

Channels are 20 nm in depth while width is 2 $\mu$m with constant length of 500 $\mu$m. As declared from the manufacturer, channels surface roughness was less than 1 nm and the contact angle measured 18 ± 8°. Fluidic connections were purchased from Upcharch Scientific, USA. Borosilicate glass syringes equipped with PEEK connectors were purchased from ILS (Innovative Labor System, Germany). Microcapillaries were used to connect the syringes to the chip. We performed FCS on Rh6G ($M_W$ = 479; Fulka, Sigma Aldrich). DI water (pH = 6.3, 18 MΩcm$^{-1}$) filtered with 100 $\mu$m filters (Whatman), as to avoid dust clogging in the reservoirs, was used to prepare fresh solutions. A confocal fluorescence correlation spectroscope, ConfoCorII (Carl Zeiss, Jena, Germany) was used to carry out FCS experiments. A 488 nm laser beam was focused by a Apochromat 63× water immersion objective (numerical aperture of 1.2); the emitted fluorescent light was collected by the same objective and separated from the excitation light by a dichroic mirror. The emission beam was mapped onto a pinhole (70 $\mu$m) in the image plane of the objective. Fluorescent emission was sent to a 530 nm LP and then acquired on the avalanche photodiode (APD).

Fluorescence was detected by an APD in single-photon-counting mode. The system built-in correlator was employed for bulk measurements, though a custom developed software (Fluctuation Analyzer) was dedicated to the analysis of measurements in microconfinement. Channels were placed in a custom designed chipholder. Chips were connected by PEEK connectors to a syringe filled with solution, preconditioned with DI water, and then loaded with a 100 nM solution of fluorescent molecules. A small pressure was applied, and the solution was sucked into the reservoirs; then, when no residual flux was registered, microcapillaries were connected in order to prevent evaporation from reservoirs. Channels were let to equilibrate at 23°C overnight before measurements to permit the fluorescent solution to diffuse from the reservoirs to the channels, which were previously imaged for control.

In order to minimize artifacts due to focus positioning with respect to the channel height, focus was positioned in correspondence to the maximum molecular brightness and performed in the middle of channels to demonstrate laser beam lateral confinement. All ACFs were calculated directly from signal trajectories acquired with a bin time of 1 $\mu$s. To optimize computer performance, data were further binned during analysis to 10 $\mu$s. The maximum lag time was set to 30 s for bulk measurements and to 300 s for channel measurements. The translational diffusion time was obtained from the autocorrelation function of the intensity fluctuations monitored as a function of time. Focal volume parameters were fit from ACF curves of 10 nM Rh6G dye diffusing in water (diffusion coefficient $2.8 \times 10^{-6}$ cm$^2$s$^{-1}$) and eq 3 to obtain $r_{xy}$ which measured 0.15 $\mu$m.

## RESULTS AND DISCUSSION

FCS is widely used for concentration and mobility measurements of fluorescent probes in biological systems like cells and plasma membranes. Whenever FCS is carried out in small systems of comparable or smaller size than the focal volume, deviations from the conventional ACF may be registered. In these cases, the validity of the standard model is weak since boundary effects become relevant. In confined compartments, erroneous results in terms of both molecule concentration and characteristic diffusion time could be obtained inducing misconceptions about the real physics governing mass transport. For this reason, we developed an ACF model which explicitly accounts for the presence of confinements on the confocal volume length scale. We demonstrated that the reflection and superposition method can successfully account for the confinement effect and well describe the generally attended physics behavior. We pointed out that the only presence of walls has a severe effect on the ACF shape which strongly deviates from the standard model. Moreover, we identify a characteristic time, $t_R$, at which the deviation takes place. This characteristic time is directly correlated with the system width through the dimensionless parameter, *R*. We showed that $t_R$ increases with increasing system size.

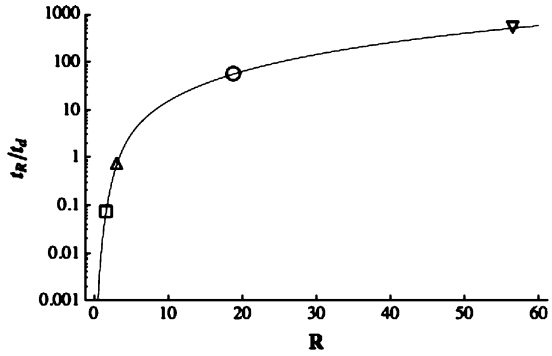


**Figure 5.** Ratio of $t_R$ and $t_d$ as a function of system size, $R$. The ratio is almost equal to 1 for $R$ close to 3.5. $t_R$ becomes larger than $t_d$ at increasing system size, $R$, and the wall effect becomes progressively negligible. Experimental results analyzed are shown on the curve: $t_R/t_d$ close to 0.1 was found in 0.35 $\mu$m channels (square); in 0.6 $\mu$m channels, a time ratio of about 1 was measured (triangle up), whereas in 2 $\mu$m channels the ratio is several times larger than 1 (circle). In 10 $\mu$m channels, the $t_R$ value is more than 2 orders of magnitude larger than $t_d$ (triangle down) and the system recovers completely an infinite size along the confined length.

At this point, it is crucial to identify the relationship between $t_R$ and $R$, which can be derived by defining $t_R$ as the lag time at which the standard ACF becomes equal to the plateau value of the confined ACF at that $R$ size; see Figure 3a, obtaining the following expression,

$$t_R = t_d\left(1 - R^2\frac{\mathrm{erf}(R/\sqrt{2})^2}{2\pi\mathrm{erf}(R/2)^4}\right) \qquad (12)$$

The ratio of $t_R$ and $t_d$ sharply increases with $R$ for $R$ less than 20; see Figure 5. In this range, the confinement exerts the highest effect on the ACF, whereas for larger $R$ values, $t_R$ becomes 2 orders of magnitude bigger than the characteristic diffusion time, $t_d$, locating the deviation at the ACF value not readily detectable by the FCS setup.

In order to validate the proposed model, we picked out ACF data from literature and performed FCS experiments in channel of micrometric width. Indeed, several authors[6,7] investigated probe mobility inside nanochannels of micrometric and submicrometric widths, and they all registered deviations from the standard ACF model. Commonly, these experiments were carried out in channels of nanometric height, thus resulting in the $g_z$ correlation contributing a negligible amount. Therefore, they were all interpreted by 2D ACF models. In these particular cases, the channel heights were all several times larger than the probe size which assured that the probe lateral mobility was unaffected by the topological confinement exerted by the nanometric extent of the channel height.[20] Therefore, the probe mobility is attended to be unchanged in micrometric wide channels as well. In particular, the 2D standard ACF model well represented the experimental behavior in channels having width of 10 $\mu$m independently from the specific experimental conditions adopted. This evidence is well explained by our model. In fact at $R$ corresponding to 10 $\mu$m confinement, the $t_R$ value is about 3 orders of magnitude larger than $t_d$, thus making the technique insensitive to this confinement grade;

(20) De Santo, I.; Causa, F.; Netti, P. A. *Anal. Chem.* **2010**, *82*, 997–1005.

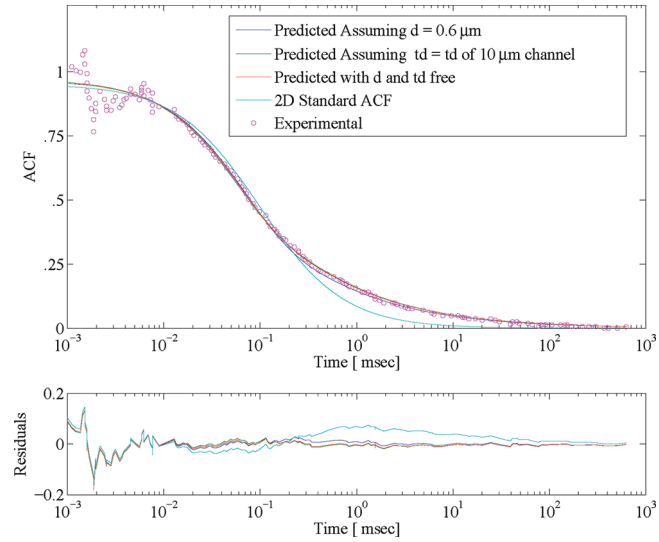


**Figure 6.** Fluorescence autocorrelation curve measured in the center of a 0.6 $\mu$m wide channel filled with 10 nM solution of Alexa 546 in water; the autocorrelation was fit to the 2D ACF model accounting for confinement in one dimension. The fitting predicted channel width and characteristic decorrelation time is equal to 0.56 $\mu$m and 80 $\mu$s, respectively. This result is in agreement with the value of 77 $\mu$s obtained by the standard model for a larger channel of 10 $\mu$m width, in the same operative conditions.

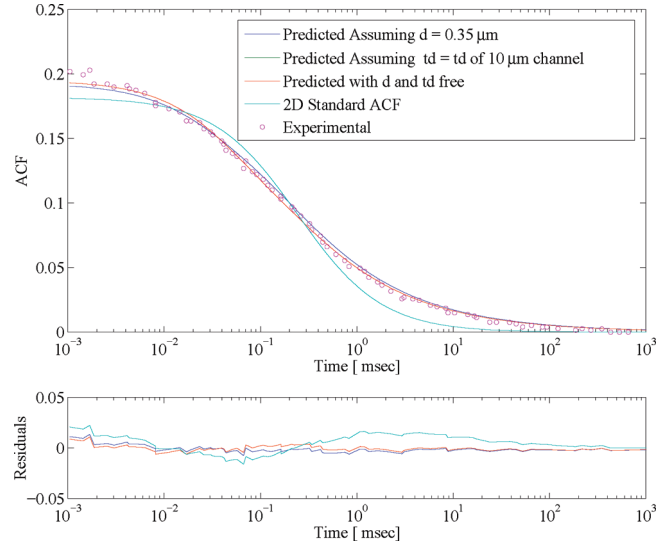


**Figure 7.** Fluorescence autocorrelation curve measured in the center of a 0.35 $\mu$m wide channel filled with 1 $\mu$M solution of Alexa Fluor 488-5-dUTP in water; the autocorrelation was fit to the 2D ACF model accounting for confinement in one dimension. The fitting predicted channel width and characteristic decorrelation time is equal to 0.4 $\mu$m and 103 $\mu$s, respectively. The predicted characteristic time is equal to the one obtained by the 2D ACF standard model for a larger channel of 10 $\mu$m width, in the same operative conditions.

see Figure 5. On the other hand, whenever the confinement grade was on the focal volume length scale, the 2D standard model was unable to predict the ACF and relevant deviations were reported.

Petrásek et al.[7] performed ACF measurements of Alexa 546 water solutions in silicon oxide channels of different sizes detecting large deviations from the 2D standard model in channels of 0.6 $\mu$m width, which is about two times the horizontal length of the focal volume. They reported that 2D or 1D standard models were unable to provide physically reasonable probe mobilities in

the channels. To account for these deviations, the authors used the model proposed by Gennerich.[10] Their analysis gave a characteristic time of 98 ± 7 $\mu$s, slightly higher than the one measured in wider channels of 10 $\mu$m width (77 ± 3 $\mu$s), and a channel width esteem 40% bigger than the nominal value.

Then, our model was used to fit the ACF recorded in 0.6 $\mu$m wide channels under several assumptions as shown in Figure 6. First, the mobility was kept unchanged with respect to the one measured in 10 $\mu$m wide channels, and the channel width was estimated as a unique unknown parameter. This procedure yielded a channel width of 0.55 ± 0.03 $\mu$m with 8% deviation with respect to the nominal channel size. Instead, assuming the channel width is equal to its nominal size (0.6 $\mu$m) and the mobility is unchanged along the unconfined direction (77 $\mu$s), a $t_d$ value of 90 ± 13 $\mu$s was estimated along the channel width. Considering both $t_d$ and $R$ as unknown parameters, a channel width of 0.56 ± 0.05 $\mu$m and a $t_d$ value of 80 ± 6 $\mu$s were evaluated. The proximity of all estimated values proves that mobility and confinement extent can be simultaneously evaluated. The larger $t_d$ value of 90 $\mu$s along the channel width could be due to molecule−wall interactions which are not explicitly accounted for in this model and can result in an apparent reduced mobility. This effect will be considered in an extended version of the confined model proposed.

Foquet et al.[6] measured Alexa Fluor 488-5-dUTP mobility in nanochannels of different widths by FCS. They also reported an ACF deviating from the 2D standard model in narrow channels. Again the 2D standard model could interpret the results for a 10 $\mu$m wide channel, giving $t_d$ of 103 ± 2 $\mu$s, but failed when applied to an ACF recorded in a 0.35 $\mu$m wide channel estimating a $t_d$ of 244 ± 4 $\mu$s (see Figure 7). When $t_d$ was kept equal to the value found in 10 $\mu$m wide channels, our confined model was then adopted to identify the confinement extent obtaining 0.40 ± 0.02 $\mu$m. Such good esteem is still found when both fitting parameters, $t_d$ and $R$, are let free, giving the same values calculated before within confidence intervals.

After validating our model on already available data sets on a submicrometric wide channel, we measured Rh6G diffusion in channels of 20 nm height and 2 $\mu$m width, Figure 8. The 2D standard model gave a $t_d$ of 24 ± 2 $\mu$s compared with 20 ± 2 $\mu$s measured in bulk experiments. When the nominal channel width as a confinement value is imposed, a $t_d$ of 29 ± 1 $\mu$s was obtained, whereas assuming the mobility unchanged with respect to the bulk, a channel width of 0.76 ± 0.07 $\mu$m was evaluated. In our case, the 2D standard model deviates from the experimental ACF only at large lag time values. This deviation occurs later with respect to former cases since the channel is now several times larger than those used in previously reported experiments. This implies that the standard model results are still reasonable at this confinement grade. Anyway, our model well interprets ACF at large lag time as shown in the residual plot in Figure 8. However, the combination of small diffusion time and large lateral width causes a weak independent parameter estimation due to the deviation occurrence on a noisy part of the ACF.

The proposed model provides reliable results both for submicrometric and micrometric confinements. In Figure 5, all analyzed experiments are reported in terms of their corresponding dimensionless parameter $R$. In the range investigated by Petrásek, both 1D and 2D standard ACF models were unable to interpret correctly the ACF data, since the average time between sequential particle−wall collisions is comparable with $t_d$. At higher confinement grades, such as those considered by Foquet, the $t_R/t_d$ ratio is close to 0.1 and the deviation from the standard 2D model occurs on the early part of the ACF. The results of our model properly predict the diffusion time and the confinement grade although the system dimensions are reaching the sensitivity limit below which also the ACF lateral direction contribution becomes negligible, hence approaching a 1D system. This implies that the limited size of the confocal optics determines the lower bound applicability limit of our model. On the other side, in the experimental conditions we investigated, the Rh6g $t_R$ attains a value 1 order of magnitude larger than $t_d$. Here, channel dimensions are large enough to achieve still reasonable results with the 2D standard model. Therefore, fast diffusing probes can be employed for the investigation of microstructured cavities having dimensions up to a few micrometers. Overcoming these length scale model results are no longer reliable, and other methods might become more appropriate in material characterization.

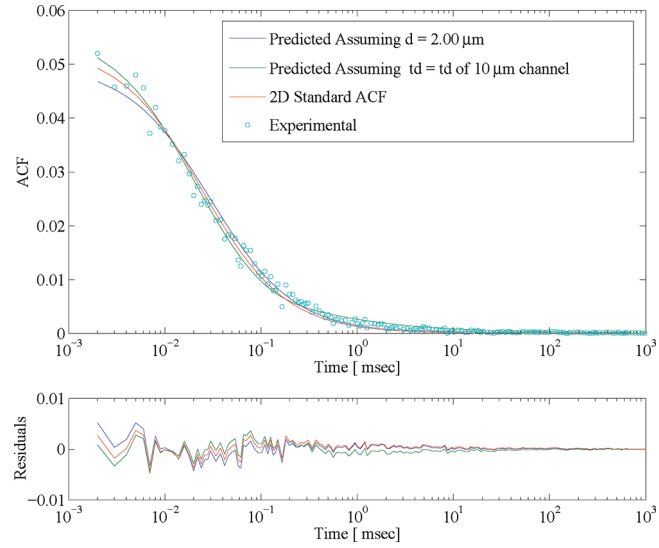


**Figure 8.** Fluorescence autocorrelation curve measured in the center of a 2 $\mu$m wide channel filled with 10 nM solution of Rh6G in water; the autocorrelation was fit to a 2D ACF model accounting for confinement in one dimension. When the nominal channel width as confinement value is imposed, a $t_d$ of 29 $\mu$s was obtained in agreement with 20 $\mu$s measured in bulk experiments.

Additional considerations are needed for the interpretation of an ACF generated in confined systems. Freely diffusing probes are commonly considered isotropic in motion. This assumption is reasonable measuring fluorescent probe mobility in homogeneous infinite systems but becomes weak when diffusion takes place in anisotropic systems of diverse lengths on the same length scale of the focal volume size.

Figure 9 shows a 2D channel of finite extent along the $\hat{y}$ axis and infinite size along the $\hat{x}$ axis, and the MSD evolution of a probe initially located at the channel center where the laser is focused. The inset represents the most relevant elements of the trajectory ensemble upon which ACF is computed. As far as the probe freely moves along both directions, the $g_y$ and $g_x$ contributions are

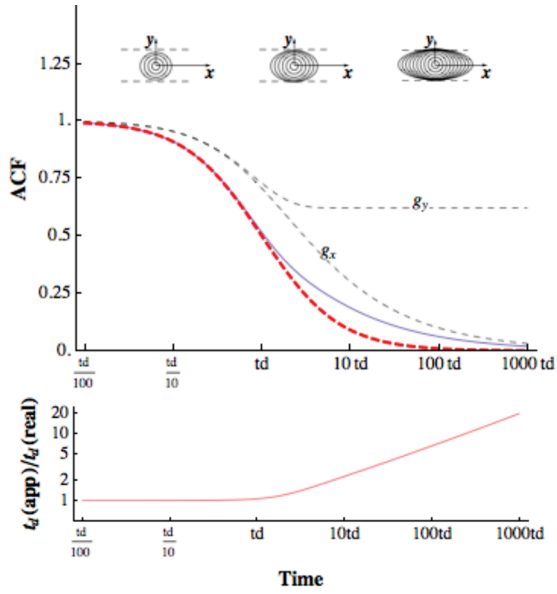


**Figure 9.** Apparent time dependent mobility in FCS experiment explained by means of MSD confinement. The inset shows MSD profiles in a 2D system constrained along the $\hat{y}$ direction. When the MSD contribution along the confined direction becomes comparable with the squared lateral confinement, the ACF (blue full line) deviates from the 2D standard model (thick dashed red line). At the point where the deviation from the standard model occurs, the apparent characteristic time (red full line) starts to increase with a power law time dependency.

equal, thus resulting into a 2D standard ACF. This condition is fulfilled until the MSD becomes comparable with the lateral confinement square size, thus approaching its maximum value along the confined axial direction, $\hat{y}$. From this point onward, the decorrelation rate along the $\hat{y}$ direction begins to diminish until it becomes zero when the maximum MSD value is reached. This causes the ACF to deviate from the standard model and a decorrelation slowdown as caused by a probe mobility reduction. In order to quantify this apparent probe mobility reduction, we compare the 2D standard ACF with our model, thus obtaining the following expression for the apparent $t_d$

$$t_{d(app)} = t\frac{g_x g_y}{1 - g_x g_y} \tag{13}$$

Figure 9 shows the apparent mobility trend for a system having a lateral extent corresponding to the dimensionless parameter $R$ equal to 4. At the lag time where the deviation takes place, the diffusion time sharply increases with a power law time dependency; see Figure 9. In confined conditions, this trend may arise on detectable lag times if characterized by $t_R$ values lower than $t_d$. In these conditions the ACF shape could reasonably be assimilated to anomalous-like transport mechanisms. Especially in these particular cases, neglecting the walls effect could lead to erroneous results.

It is worth noticing that the proposed model provides the capability of reformulating the confined ACF in terms of its unconfined equivalent. These methodology results are general and still applicable to cases in which the diffusion is not ideal or occurs simultaneously with other phenomena, i.e., reaction or adsorption and sticking at the walls. Moreover, the proposed approach allows one to remove all assumptions regarding the shape of the detectivity function since the line scanning profiles can be used to directly determinate the $a_n$ coefficients in eq 6 by fast Fourier transform (FFT). The detectable emission intensity distribution should anyway be precisely described in order to assess molecular mobility in systems comparable with the focal volume size.

## CONCLUSIONS

In confined systems, the ACF deviates from the standard model and the relevance and occurrence of such deviations depends on the molecule mobility and the system size. A close form solution is proposed for micrometric and submicrometric compartments having at least one dimension comparable with the characteristic detection volume length.

The proposed model allows the evaluation of such deviations and a better esteem of the parameters of interest, thus characterizing the undergoing transport process without invoking any semiempirical and numerical model. In addition, it permits the investigation of microstructured material features such as cages and cavities having dimensions on the micrometric range. In particular, we measured the lateral confinement extent in a channel of micrometric width with almost 8% error. The model, thus, represents an important step toward the measurement of mass transport in confined systems by means of the FCS technique.

## ACKNOWLEDGMENT

This work has been fully granted by the Italian Ministry of Research (MIUR) project, TriPoDe (DM20160). The authors sincerely acknowledge Dr. Malte Wachsmuth for the kind gift of the Fluctuation Analyzer Software.

Received for review May 4, 2010. Accepted October 9, 2010.

AC102084M